CHEMISTRY
A EUROPEAN JOURNAL

DOI: 10.1002/chem.200700967

Formation of ZSM-22 Zeolite Catalytic Particles by Fusion of Elementary Nanorods

Kazuaki Hayasaka,[a] Duoduo Liang,[b] Ward Huybrechts,[a] Bart R. De Waele,[a] Kristof J. Houthoofd,[a] Pierre Eloy,[c] Eric M. Gaigneaux,[c] Gustaaf van Tendeloo,[b] Joris W. Thybaut,[d] Guy B. Marin,[d] Joeri F. M. Denayer,[e] Gino V. Baron,[e] Pierre A. Jacobs,[a] Christine E. A. Kirschhock,[a] and Johan A. Martens*[a]

Abstract: An ZSM-22 aluminosilicate zeolite was synthesized using the hydrothermal gel method at 150 °C. Products obtained after different synthesis times were characterized using various techniques and catalytic testing. Massive formation of ZSM-22 nanocrystals occurs after only a short synthesis time, appearing as isolated rods with a cross section of 12 ± 4 nm. Nanorods have aluminum enriched at their external surface. Later in the crystallization process nanorods align and fuse sideways, whereby the external surface is systematically converted into an internal micropore surface. The formation of aluminum bearing micropores by the joining of nanorod surfaces is responsible for the enhanced catalytic activity. For this, the zeolite synthesis of nanoscale crystallites is ineffective for enhancing catalytic activity.

Keywords: aggregation · aluminum · crystal growth · microporous materials · zeolites

Introduction

Zeolite nanocrystals that have particle sizes smaller than 200 nm are useful for the preparation of zeolite films,[1–3] membranes[4,5] and hierarchical materials.[6–12] In the field of catalysis, particle size generally is considered to be an important parameter for tuning the activity and selectivity of a zeolite catalyst.[13] The shortening of the channels in nanoscaled zeolite particles can lift the diffusional limitation of the reaction rate often encountered in micron size zeolite crystals. Nanozeolites are conveniently synthesized from monomeric silicon sources in the presence of high concentrations of an organic template.[14–24] The key for reducing the zeolite particle size limitation is to favor nucleation over crystal growth. This effect can sometimes be achieved by applying a special temperature profile during crystallization.[25–27] For instance, in the synthesis of nanosize Silicalite-1, long ageing times at room temperature followed by fast heating provokes massive formation of nanocrystals.[25,26] Departing from polymeric silicon sources the hydrothermal gel method for zeolite synthesis, when adapted for nanocrystal synthesis, generally results in difficult to separate aggregates.[14] Such aggregates of elongated nanoparticles are encountered with zeolites that have TON framework topology[28] called ZSM-22, Theta-1, KZ-2, ISI-1 and Nu-10.[29–39] The basic component of these zeolite particles was identified as a rod with a nanosize rectangular cross section.[35]

TON type zeolites are valuable catalysts for petrochemical processes such as hydroisomerization dewaxing[41] and propene oligomerization.[42] The TON framework topology is characterized by a monodimensional 10-membered ring

[a] K. Hayasaka, Dr. W. Huybrechts, Dr. B. R. De Waele, K. J. Houthoofd, Prof. P. A. Jacobs, Prof. C. E. A. Kirschhock, Prof. J. A. Martens
Centre for Surface Chemistry and Catalysis
Catholic University of Leuven
Kasteelpark Arenberg 23, B-3001 Leuven (Belgium)
Fax: (+32) 16-32-19-98
E-mail: johan.martens@biw.kuleuven.be

[b] D. Liang, Prof. G. van Tendeloo
EMAT, Electron Microscopy for Materials Science
Department of Physics, University of Antwerp
Groenenborgerlaan 171, B-2020 Antwerp (Belgium)

[c] Dr. P. Eloy, Prof. E. M. Gaigneaux
Unité de Catalyse et Chimie es Matériaux Divisés
Université Catholique de Louvain
Croix du Sud, 2 Bte 17, B-1348 Louvain-la-Neuve (Belgium)

[d] Prof. J. W. Thybaut, Prof. G. B. Marin
Laboratorium voor Petrochemische Techniek
Ghent University, Krijgslaan 281 S5, B-9000 Ghent (Belgium)

[e] Prof. J. F. M. Denayer, Prof. G. V. Baron
Department of Chemical Engineering
Free University of Brussels
Pleinlaan 2, B-1050 Brussels (Belgium)

pore system.[28] The channels run along the longest dimension of the crystals (crystallographic *c* direction).[36] TON type zeolites can be synthesized from aluminosilicate hydrogel in presence of a variety of oxygen or nitrogen containing linear organic template molecules such as amines, aminoalcohols, α,ω-diamines, long-chain polyamines, quaternary ammonium compounds, or alcohols next to alkali metal cations.[32,37,38,40] A peculiarity of the synthesis of TON type zeolites is the formation of a template rich layer around silica particles upon mixing of the reactants, and the occurrence of heterogeneous nucleation in this organophilic surface layer.[39] The final aggregate sometimes appears as aggregated nanoparticle shells of a hollow micrometer size sphere, corresponding in size to the initial gel spheres.[37] Here we report the synthesis of individual rod shaped TON nanocrystals. We investigated their properties and the evolution of the catalytic activity upon aggregation of these nanorods.

Results and Discussion

Zeolite ZSM-22 was crystallized following the protocol by Ernst et al. that involves the hydrothermal treatment of 1,6-diaminohexane and potassium containing aluminosilicate hydrogel at 150 °C.[37] Solid products were recovered after different heating times. The X-ray diffraction (XRD) patterns are shown in Figure 1a. After 14.5 hours heating the product is still largely amorphous, but already the characteristic Bragg reflections of TON framework topology emerge in the XRD pattern. The XRD intensities rise over the next few hours, rapidly increase after 26 hours synthesis time, and approach their final intensity after 38 hours. Amorphous silicate scatters in a broad signal around a *d*-value of about 3.9 Å, corresponding to Si–Si interatomic distances.

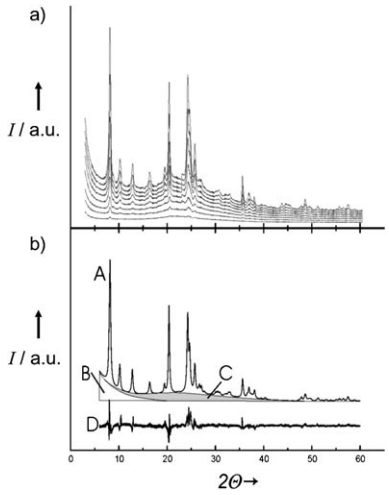

Figure 1. a) X-ray diffraction patterns of ZSM-22 samples after different synthesis times: spectra from bottom to top: 14.5, 22, 26, 28, 30, 38, 46, 58 h. b) Example of refined data (after 38 h synthesis): A: simulated pattern; B: decay of low angle scattering; C: amorphous background; D: difference between experimental and simulated data.

The Bragg crystallinity relative to the finally obtained product after 58 hours (defined as 100 % crystallinity) was derived from the ratio of integrated Bragg reflections and amorphous scattering (Figure 1b and 2b). Particle width *D*

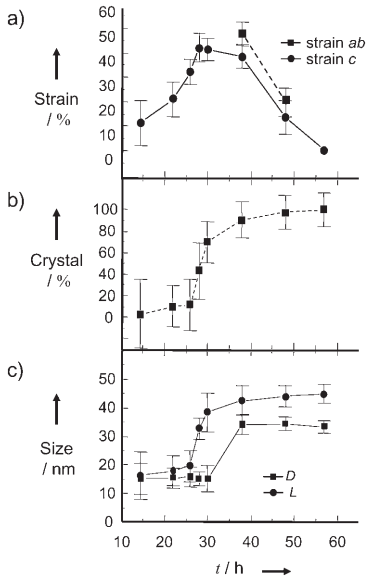

Figure 2. a) Strain of the ZSM-22 crystallites derived from XRD, b) crystal dimensions, and c) crystallinity. Error bars are derived from the estimated standard deviation of the refined profile and background parameters.

(in the *a* and *b* crystallographic directions), length *L* (in the *c* direction), intracrystalline strain in the needle-direction (*c* direction), and perpendicular to it (*a* and *b* direction) were obtained from the Rietveld refined profile parameters (Figure 2a,c). The initially observed TON crystallites after 14.5 hours synthesis measured 15 ± 5 nm in all three dimensions (Figure 2c). This closely resembles the size of the original sol particles of the colloidal silica source. According to XRD, in the period from 14.5 to 30 hours the crystals preferably grew in the direction of the pores, that is, the *c*-direction, to reach a length *L* of 38 ± 8 nm at almost constant diameter *D* of 15 ± 5 nm (Figure 2c). In the period from 30 to 38 hours the aspect of the particles significantly changed: the elongated particles suddenly widened to a *D* value of 35 ± 5 nm, while lengths further increased only little (Figure 2a). This sudden change of the main growth direction from *c* to *a* and *b* after 30 hours suggests a change of growth mechanism.

The solid product yield varied little with synthesis time and amounted to 95 ± 3 % of the silica and alumina introduced into the autoclave. The crystallinity of the zeolite product increased from 70 ± 15 % after 30 hours to 90 ± 10 % after 38 hours (Figure 2b). During this period the nanorods grow by about 15 % (from $L=38\pm8$ nm to 43 ± 5 nm) and more than double in width *D* (from $D=15\pm5$ to $D=35\pm5$ nm, Figure 2c). This relates to an approximate increase of individual particle volume by more than 500 %.

The experimentally observed gain of crystalline zeolite yield by roughly 20% can not account for this increase of the particle size. Sideways fusion of still growing nanorods, however, can directly explain the sudden change of particle width and the more gradual increase of particle length. Ostwald ripening was considered as an alternative explanation for the increase of the size of the suspended particles, but the uniformity of the original nanorods width ($D = 15 \pm 5$ nm) makes Ostwald ripening an unlikely explanation as such mechanisms requires a variation of size. Later than 38 hours the system enters an annealing phase (Figure 2c). Strain within the particles is reduced without much change of neither particle size nor aspect (Figure 2a). The outcome of the XRD results is summarized in Figure 3 and Table 1.

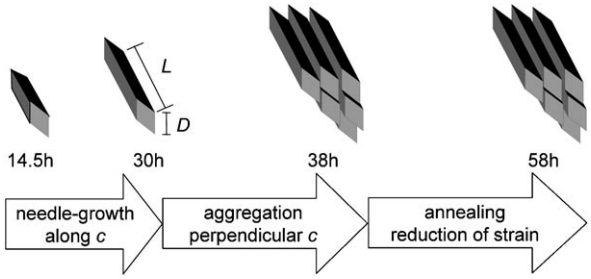

Figure 3. Progression of the ZSM-22 zeolite synthesis.

Table 1. Interpretation of the ZSM-22 sample series according to XRD, TEM and N_2 adsorption.

Synthesis time [h]	N_2 D [nm]	TEM D [nm]	TEM L [nm]	XRD D [nm]	XRD L [nm]
14.5	–	–	–	15	15
30	20	12[a]	40–60	15	40
38	35	–	–	35	45
46	35	–	–	–	45
58	50	35	40–60	35	45

[a] [200] and [110] fringes only.

SEM pictures of 30 and 58 hours samples show clustered, elongated particles with thicknesses around 40–100 nm and lengths in the micron scale (Figure 4). Asides the degree of clustering, no marked differences in morphology of the two samples are observed by scanning electron microscopy (SEM). This morphology is typical of ZSM-22 and related zeolites.[34] The particle sizes according to SEM are larger than estimated from XRD.

Sizes obtained by profile analysis of powder XRD data are related to almost single-crystalline regions within the particles observed with SEM. The crystallite sizes and the hypothesis of aggregation were further investigated with transmission electron microscopy (TEM). A detailed TEM analysis was performed on samples collected after 30 and 58 hours. As already observed by XRD, after 30 hours the product is crystalline (Figure 5a). A TON type zeolite is present as a large amount of nanorods with an average width D of 12 ± 2 nm (Figure 5d). Fringes proving that crystallinity can be assigned in cases of favorable orientation to the electron beam. Only two lattice directions perpendicular

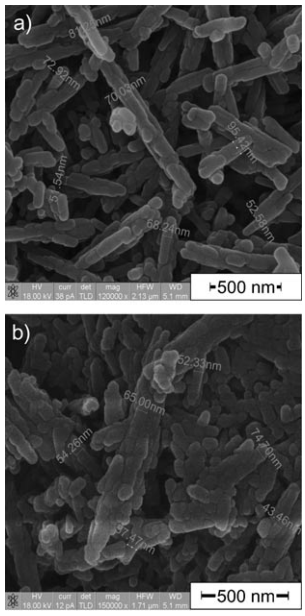

Figure 4. SEM of ZSM-22 zeolite after a) 30 h and b) 58 h of the synthesis.

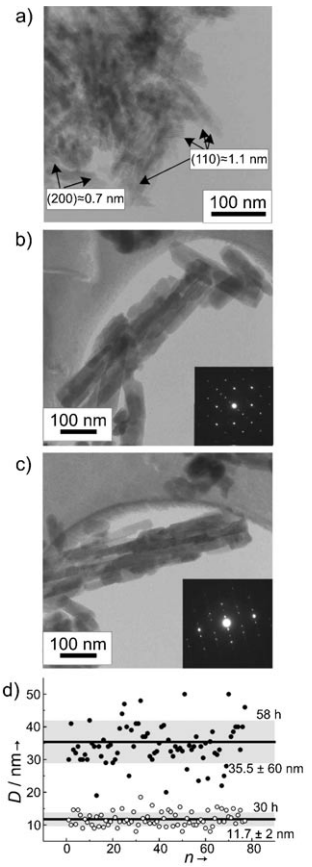

Figure 5. TEM of a) 30 h, b,c) 58 h sample, and d) reading of crystallite width at the respective times. Mean values are indicated by lines, the standard deviation as grey bars.

to the needle axis could be observed, namely the [200] and the [110] direction (Figure 5a). Often needles with the same orientation were found in close proximity and parallel to each other. The rods are bunched together, which makes the measurement of their length difficult. Where length could be estimated, 40 to 60 nm often was observed in the 30 hours sample. Some isolated needles were up to 100 nm long. The final product (58 hours) appears at first sight in the TEM analysis, to be like an up-scaled version of the sample obtained after 30 hours (Figure 5b,c). Closer inspection, however, revealed that the elongated particles are made up from the thinner nanorods observed before in the 30 hours sample. The sharp spots of the diffraction patterns (Figure 5b,c) of such an aggregated particle reveal the excellent alignment of the nanorods in the *a* and *b* direction before fusion and annealing into the final product. According to our TEM measurements the final width *D* after 58 hours synthesis is 35 ± 5 nm (Figure 5d). XRD correctly describes the thicknesses of the particles measured using TEM (Figure 3 and Table 1), whereas the length observed with TEM appears to be slightly larger than the value obtained by XRD. TEM and XRD both strongly support a growth model of TON zeolite, where at first nanorods grow into rod-direction until the medium is almost depleted. Later nanorods fuse in an aligned manner (Figure 3).

The texture of the intermediate and final samples was characterized by using nitrogen adsorption at $-196\,^{\circ}C$. The surface area of a zeolite particle consists of internal surface of the zeolite micropores and external surface on the outside of the particle. The evolution of microporosity, Brunauer, Emmett, and Teller (BET) surface area, and external specific surface area of the calcined samples are shown in Figure 6. The total BET specific surface area in the initial period from 14.5 to 26 hours is $\approx 60\,m^2\,g^{-1}$. It rises above $200\,m^2\,g^{-1}$ within the next two hours and remains high in later samples. The specific external surface area originally is smaller than $50\,m^2\,g^{-1}$. In the period 28 to 30 hours where isolated nanorods are formed (Table 1 and Figure 3), the external surface area rises sharply and reaches a maximum of $\approx 115\,m^2\,g^{-1}$. At later times, the specific external surface area of the particles decreases again, whereas the microporosity increases (Figure 6b). The final sample has a microporosity of $\approx 87\,\mu L\,g^{-1}$. These textural changes upon aggregation of the nanorods into final crystals were modeled following the approach by Aguado et al. developed for ZSM-5 aggregation.[26] The model accounts for transformation of external surface into micropore surface through fusion of particles. According to this model, the crystal width *D* increases from 20 nm at 30 hours to 50 nm at 58 hours (Table 1). The agreement of the crystal dimensions according to N_2 adsorption with XRD and TEM is reasonable (Table 1). Micropore volume determination of nanosize zeolites is rather approximate, owing to border effects.[42] Still, the relative increase of the crystal width *D* by a factor of 2.5 in the period from 30 to 58 hours, derived from N_2 adsorption, is in very good accordance with XRD and TEM (Table 1).

The average Si/Al ratio of the time series of zeolite samples determined by chemical analysis was around 30 and varied little with synthesis time (Table 2). It corresponds to the Si/Al ratio of the synthesis mixture. The Si/Al ratio at the surface of the particles determined by using X-ray photoelectron spectroscopy (XPS) (Table 2) was shown to be much lower, and increased from 10.7 at 26 hours to 17.2 at 58 hours. XPS reveals that the aluminum is concentrated in the rim of the particles. Considering that the penetration depth of the XPS analysis is of the order of a few nanometers, the ZSM-22 particles must be fairly siliceous in their interior and have aluminum concentrated on their external surfaces. The ^{27}Al MAS-NMR spectra of the series of samples are shown in Figure 7. Originally, when the solid is still largely amorphous (14.5 and 26 hours) the ^{27}Al NMR signal is substantially broadened. The NMR signal sharpens and displays a maximum around 53 ppm after 28 hours and later. This chemical shift is typical for tetrahedrally coordinated framework aluminum. Recent investigations on aluminum siting in TON type zeolites by means of NMR techniques revealed a preferential population of T3 and T4 sites.[43] Especially the T4 sites located in lobes of the main pore (Figure 8c) are prime candidates for aluminum posi-

Table 2. Characterization of ZSM-22 samples with chemical analysis, XPS, and catalytic testing.

Synthesis time [h]	Si/Al (chem. anal.)	Si/Al (XPS)	Apparent reaction rate [$mol\,kg^{-1}\,s^{-1} \times 10^{-6}$]
26	30.0	10.7	8.3
28	31.3	12.8	22.3
30	31.2	15.5	27.8
38	29.9	15.5	66.6
46	-	-	53.5
58	30.6	17.2	77.5

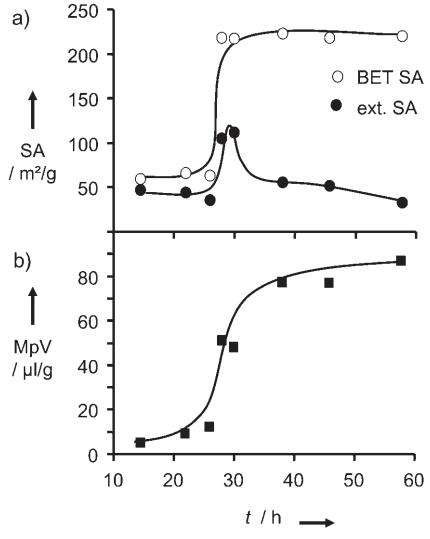

Figure 6. Texture of ZSM-22 sample series: a) BET specific surface area (SA) and specific external (ext.) SA and b) the specific micropore volume.

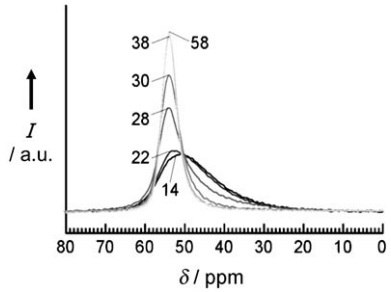

Figure 7. ^{27}Al MAS-NMR spectra of ZSM-22 sample series. Synthesis times (in hours) are indicated (14–58 h).

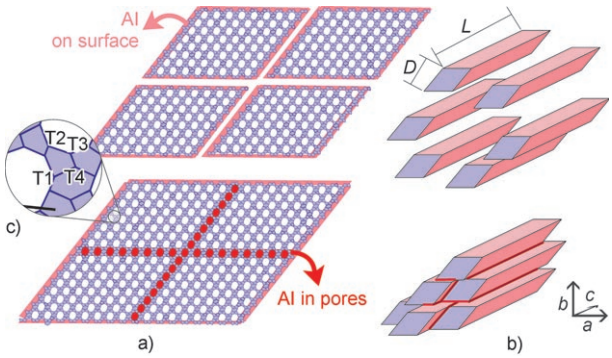

Figure 8. Model of ZSM-22 nanorod aggregation. a) Aggregation of nanorods, b) formation of intergrowth of nanorods, and c) adopted T-atom siting.

tions. Even when present at the surface of a crystal boundary, these sites can have four linkages to other T sites, which is in agreement with the Al(4Si) environment observed by ^{27}Al magic angle spinning NMR (MAS-NMR) (Figure 7).

The changes with synthesis time of the Si/Al ratio according to XPS (Table 2) can be explained by the proposed aggregation model. A representative molecular model of $D\times D$ faces of 4 aggregating nanorods with a D value of $\approx$13 nm is depicted in Figure 8a. One such nanorod has 90 micropores, 20 half-micropores on the (110) face and 18 half-micropores on the (100) face. Sideways linking of this array of 2×2 nanorods to compose the aggregate, results in one wider particle with 38 new micropores that did not exist in the individual nanorods.

The increase of surface Si/Al ratio in the synthesis time period from 30 to 58 hours from 15.5 to 17.2 (Table 2) reflects an increased relative exposure of siliceous faces as a result of aggregation. According to XRD and TEM, the nanorod aggregation involves mainly lateral $D\times L$ surfaces, and less the $D\times D$ faces (Figure 3). This infers aluminum to be preferentially positioned in the lateral surfaces ($D\times L$) of the nanorods.

The series of ZSM-22 samples were converted into bifunctional catalysts and characterized by means of decane hydroconversion. The ZSM-22 nanorods taken from the 30 hours sample were substantially less active than the annealed samples obtained at 38 hours and later times (Table 2). This observation opposes the general idea that reduction of the zeolite particle size to the nanometer domain leads to superior catalytic performance. In this particular case, the gain in catalytic activity can be explained by the higher activity of the Al-sites within a zeolite pore compared to the Al on the exterior surfaces. Owing to the conversion of external to internal Al by nanorod aggregation, the catalytic activity of ZSM-22 is increased after the nanorods are fused.

The refined constraint index (CI°) reveals the shape selectivity of a zeolite.[44] The higher this index, the more catalysis that occurs in the micropores. Medium-pore zeolites have CI° values higher than 2.2.[44] The CI° value jumps from around 5 for isolated nanorods (30 hours) to 18 for aggregates (38 hours and later samples). This observation is in accordance with the increased number of confined acid sites, which is in turn in accordance with the aggregation model (Figure 8b).

Conclusions

This work revealed that the crystallization of ZSM-22 is a two step process. First, the gel is converted into nanorods that have the ZSM-22 type framework structure. In a second phase, nanorods align and fuse mostly through their lateral surfaces. The aggregation model is supported by XRD, TEM and N_2 adsorption. XPS reveals a non-uniform Al distribution. Aluminum is concentrated in the mantle of the nanorods. Upon lateral fusion of nanorods, external surfaces become internal, enhancing this way catalytic activity and molecular shape selectivity. A surprising consequence of the aggregation is a very special aluminum siting. In the final crystals, Al-containing pores are formed by perfect alignment and fusion of the original nanorods. Such a mechanism can have significant implications as it offers unprecedented tools for spatial organization of many kinds of functions.

Experimental Section

Synthesis of ZSM-22: Solutions of $Al_2(SO_4)_3\cdot18H_2O$ (1.33 g) in water (5 mL), KOH (1.94 g) in water (6.75 mL), and 1,6-diaminohexane (4.18 g) in water (32.5 mL) were prepared. Separately, Ludox-AS40 (18 g) was diluted with water (31 mL). The solutions containing $Al_2(SO_4)_3\cdot18H_2O$ and KOH were combined under stirring, afterwards the diluted diaminohexane was added. This mixture was then added to the Ludox. The components of the synthesis mixture have a molar ratio of 1,6-diaminohexane/K_2O/Al_2O_3/SiO_2/H_2O, 18:9:1:60:2400. An amount of 0.25 g of ZSM-22 powder from a previous synthesis was added as a seed. Synthesis gels with identical composition were prepared and poured into 8 stainless steel autoclaves with a capacity of 120 mL, which were mounted in an electric oven equipped with a rack for the tumbling of autoclaves at $\approx$60 rotations per minute. The temperature was set to 150 °C. At different times between 14.5 to 58 h, an autoclave was removed from the oven and cooled by submersion in cold tap water. The solid product was separated from the liquid by filtration, washed and dried. The organic template was removed through calcination. To this purpose, samples

were loaded in a reactor tube, heated from room temperature to 400 °C under a nitrogen flow. After 6 h the temperature was ramped with 5 °C min^{-1} to 550 °C under oxygen flow. Calcined zeolite was ammonium exchanged in the presence of an 0.5 N NH_4Cl aqueous solution under reflux conditions.

XRD: Powder diffractograms were recorded with a Stoe Stadi P diffractometer in transmission mode over the range between 3 and 60° 2Θ. Focused monochromatic $Cu_{k\alpha 1}$ radiation was used on capillaries with outer diameter of 0.5 mm.

Rietveld refinement of all patterns was performed to obtain particle size-distributions and a measure for crystallinity of the solids. GSAS software package was used for the Rietveld refinement.[45] All samples could be refined by using the atomic coordinates for TON in the space group $Cmc2_1$. Framework coordinates were calculated based on the T-coordinates listed in the Atlas of Zeolite Framework Types.[27] The nomenclature used varies from the Si-positions published by Marler et al. insofar that T1 corresponds to Si3, T2 to Si4, T3 to Si1, and T4 to Si2.[33] Oxygen positions were calculated with the program Kriber.[46] The lattice was optimized with the DLS-77 code.[47] The obtained atomic positions are in excellent agreement with the experimental coordinates.[33] Atomic parameters were not refined. To obtain comparable data for particle size broadening and avoid possible coupling of profile parameters, the reflection profiles were assumed to be Lorentzian only.[48] The particle anisotropy was accounted for by using the anisotropic broadening option of GSAS in [001] direction. This way particle sizes in the needle direction (*c*-direction) and perpendicular to it could be obtained from the refined profile parameters.[45] The refined linewidths were considerably larger than the previously determined instrumental broadening values. A correction for instrumental broadening, therefore, was not carried out. The obtained profile parameters directly correspond to the full width at half maximum (FWHM) broadening, owing to size and strain and were used to obtain the particle properties. Using the FWHM instead of the integrated width leads to an over-estimation of the particle size and an under-estimation of internal strain by as much as 57% in the case of a pure Lorentzian reflection profile. As the experimental profile shape is a combination of Gaussian and Lorentzian contributions the error is estimated to be in the range of maximally 20%. Particle sizes were calculated assuming a Scherrer constant of 1, which probably reduced the error of particle size to smaller values. Independent of the actual values, the observed trend of particle sizes reflects the true evolution of the particles aspects. All Rietveld refinements were performed until R_f^2 was smaller than 15%, with R_p usually ranging around 6%.

To assess crystallinity, that is, the amount of crystalline versus disordered alumosilicate in the solids, the intensities of Bragg reflections and amorphous background was compared for each sample. For this the powder patterns were integrated in the angle range between 6 and 60° 2Θ. Subtracting the refined background resulted in the Bragg reflection intensity. The background was then corrected for the decay of the low angle scattering and integrated. The ratio of those integrated scattering functions was used as measure for crystallinity (Figure 2b).

N_2 adsorption: The zeolite texture was characterized using nitrogen adsorption at −196 °C using an Omnisorp 100 instrument from Coulter. Micropore volume and external surface area were derived from the isotherm using the *t*-plot method. It was assumed that the 30 h sample represented isolated nanorods. Upon linking of the rods through their lateral faces, external surface area is assumed to be transformed into intracrystalline microporous surface (Figure 8a). A proportionality factor A between the specific volume V_{mic} and the BET specific surface area S_{mic} of the micropores is defined as follows:

$$V_{\mathrm{mic}} = A \times S_{\mathrm{mic}} \quad (1)$$

To determine A, a reference ZSM-22 sample with large particle size and minimum external surface area is needed. A suitable reference sample was synthesized following the same recipe but in absence of aluminum. The sample has a micropore volume of 95 μL g^{-1}, a total BET specific surface area of 182 m^2 g^{-1} and an external surface area of 7 m^2 g^{-1}. Neglecting the external surface area leads to an A value of 0.52 nm.

For the ZSM-22 samples of the synthesis time series from 30–58 h, it is assumed that the BET specific surface area comprises two contributions: external surfaces and micropores. The micropore contribution S_{mic} is calculated according to Equation (1), using the V_{mic} value obtained from *t*-plot analysis of the nitrogen adsorption isotherm. The external contribution is obtained from the resulting difference:

$$S_{\mathrm{ext}} = S_{\mathrm{BET}} - S_{\mathrm{mic}} \quad (2)$$

External surface area is assumed to vanish upon joining nanorods (Figure 8a). The change of specific external surface area S_{ext} as a result of aggregation can mathematically be expressed as:[26]

$$S_{\mathrm{ext}} = S_{\mathrm{ext,30h}}/(1+B) \quad (3)$$

in which $S_{ext,30h}$ represents the specific external surface area of the 30 h sample, and B the aggregation factor. For the 30 h sample, B is assumed to be zero.

TEM observations indicated a preferential occurrence of specific faces of the nanorods, viz. (100) and (110). This results in nanorods that have parallelogram cross sections and an angle between the edges of $\alpha = 51.6°$. For simplicity the parallelograms were assumed to be rhombical, with [100] and [110] edges to be equal in length D. Thus, the surface area of an individual rod, $S'_{ext,rod}$, corresponds to:

$$S'_{\mathrm{ext,rod}} = 4D \times L + 2\sin\alpha \times D^2 \quad (4)$$

with D and L representing the particle dimensions according to Figure 8a. Assuming D to be much smaller than L, the term $2\sin\alpha \times D^2$ can be neglected:

$$S'_{\mathrm{ext,rot}} = 4D \times L \quad (5)$$

The volume of a rod, V'_{rod}, is given by:

$$V'_{\mathrm{rod}} = \sin\alpha \times D^2 \times L \quad (6)$$

Combination of Equations (5) and (6) generates an expression for D:

$$D = 4/\sin\alpha \times V'_{\mathrm{rod}}/S'_{\mathrm{ext,rod}} \quad (7)$$

or else, expressed in specific volume V_{rod} and specific surface area S_{ext}:

$$D = 4/\sin\alpha \times V_{\mathrm{rod}}/S_{\mathrm{ext}} \quad (8)$$

The specific rod volume, V_{rod}, can be obtained as the sum of the specific micropore volume, V_{mic}, and the specific volume of the walls separating the micropores. Aguado et al. in their model for ZSM-5 nanocrystals adopted the specific volume of crystobalite (437×10^{-9} m^3 g^{-1}) for the walls.[26]

$$D = 4/\sin\alpha \times (V_{\mathrm{mic}} + 437 \times 10^{-9})/S_{\mathrm{ext}} \quad (9)$$

ICP: Zeolite samples were dissolved by using HF and HCl. From these solutions the Al content was determined using inductively coupled plasma (ICP).

^{27}Al MAS-NMR: ^{27}Al MAS-NMR spectra were recorded by using a Bruker Avance DRX400 spectrometer (9.4 T). A number of 12,000 scans were accumulated with a recycle delay of 100 ms. MAS rotors were spun at 20 kHz.

XPS: The XPS analyses were performed on a Kratos Axis Ultra spectrometer (Kratos Analytical, Manchester, UK) equipped with a non-monochromatised magnesium X-ray source (powered at 10 mA and 15 kV).

The sample powders were pressed into small stainless steel troughs mounted on a multi specimen holder. The pressure in the analysis chamber was around 10^{-6} Pa. The angle between the normal to the sample surface and the lens axis was 0°. The hybrid lens magnification mode was

used with the slot aperture resulting in an analysed area of 700 μm × 300 μm. The pass energy set at 40 eV. In these conditions, the energy resolution gives a full width at half maximum (FWHM) of the Ag $3d_{5/2}$ peak of about 1.0 eV. Charge stabilization was achieved by using the Kratos Axis device. The following sequence of spectra was recorded: survey spectrum, C 1s, O 1s, Al 2s, Si 2p and C 1s, again to check the stability of charge compensation in a function of time and the absence of degradation of the sample during the analyses. The binding energies were calculated with respect to the C−(C,H) component of the C 1s peak fixed at 284.8 eV.

The spectra were decomposed with the CasaXPS program (Casa Software, UK) with a Gaussian/Lorentzian (70/30) product function and after subtraction of a linear baseline. Molar fractions were calculated using peak areas normalized on the basis of acquisition parameters, sensitivity factors provided by the manufacturer and the transmission function.

TEM: TEM images were taken by using a Philips CM20 electron microscope (with resolution of 0.27 nm) working on 200 kV. The material was crushed and suspended in ethanol. A few drops of the solution were spread and dried on a copper grid with a porous carbon film to make a specimen.

Catalytic experiments: For catalytic experiments, ammonium exchanged ZSM-22 was impregnated with an aliquot of an aqueous $[Pt(NH_3)_4Cl_2]$ solution to obtain a Pt loading of 0.3 wt.%. Zeolite powder was compressed into a solid disc, crushed and sieved to obtain a 125–250 micrometer pellet fraction. Catalytic testing was performed on 50 mg catalyst quantities loaded in a 16 sample high throughput reactor.[49] The catalyst was activated by calcination at 400 °C in oxygen and reduction at the same temperature with hydrogen. The feedstock for the catalytic experiments was reagent grade decane (purity > 99 %). The total pressure in the reactor was 0.45 MPa, temperature was varied from 150 °C to 300 °C every 10 °C. H_2/decane molar ratio was 375 and the modified residence time 2520 kg s mol^{-1}.

Acknowledgements

The work was carried out in an IAP-PAI framework supported by the Belgian Government. J.A.M. and G.v.T. acknowledge the Flemish FWO for financial support. W.H. acknowledges the Flemish IWT for a research fellowship. K.H. acknowledges the financial support of the Japan Cooperation Center, Petroleum and Nippon Oil Corporation, for his research activities at K.U. Leuven. J.D. acknowledges F.W.O.-Vlaanderen for a postdoctoral fellowship.

[1] S. Mintova, T. Bein, *Adv. Mater.* **2001**, *13*, 1880–1883.
[2] N. Petkov, M. Hoelzl, T. H. Metzger, S. Mintova, T. Bein, *J. Phys. Chem. B* **2005**, *109*, 4485–4491.
[3] J. Choi, S. Ghosh, A. Z. Lai, M. Tsapatsis, *Angew. Chem.* **2006**, *118*, 1172–1176; *Angew. Chem. Int. Ed.* **2006**, *45*, 1154–1158 .
[4] J. Hedlund, J. Sterte, M. Anthonis, A.-J. Bons, B. Carstensen, N. Corcoran, D. Cox, H. Deckman, W. De Gijnst, P.-P. de Moor, F. Lai, J. McHenry, W. Mortier, J. Reinoso, J. Peters, *Microporous Mesoporous Mater.* **2002**, *52*, 179–189.
[5] J. Hedlund, M. Noack, P. Kolsch, D. Craeser, J. Caro, J. Sterte, *J. Membr. Sci.* **1999**, *159*, 263–273.
[6] L. Huang, Z. Wang, J. Sun, L. Miao, Q. Li, Y. Yan, D. Zhao, *J. Am. Chem. Soc.* **2000**, *122*, 3530–3531.
[7] S. Naik, A. S. T. Chiang, R. W. Thompson, F. C. Huang, *Chem. Mater.* **2003**, *15*, 787–792.
[8] Y. Liu, W. Zhang, T. Pinnavaia, *J. Am. Chem. Soc.* **2000**, *122*, 8791–8792.
[9] Y. Liu, W. Zhang, T. Pinnavaia, *Angew. Chem.* **2001**, *113*, 1295–1298; *Angew. Chem. Int. Ed.* **2001**, *40*, 1255–1258.
[10] S. P. B. Kremer, C. E. A. Kirschhock, A. Aerts, K. Villani, J. A. Martens, O. I. Lebedev, G. Van Tendeloo, *Adv. Mater.* **2003**, *15*, 1705–1707.
[11] C. S. Carr, S. Kaskel, D. F. Shantz, *Chem. Mater.* **2004**, *16*, 3139–3146.
[12] Y. Bouizi, L. Rouleau, V. P. Valtchev, *Microporous Mesoporous Mater.* **2006**, *91*, 70–77.
[13] J. Weitkamp, S. Ernst, L. Puppe in *Catalysis and Zeolites: Fundamentals and Applications* (Eds.: J. Weitkamp, L. Puppe), Springer, Berlin, **1999**, p. 327.
[14] L. Tosheva, V. P. Valtchev, *Chem. Mater.* **2005**, *17*, 2494–2513.
[15] B. J. Schoeman, J. Sterte, J.-E. Otterstedt, *Zeolites* **1994**, *14*, 110–116.
[16] A. E. Persson, B. J. Schoeman, J. Sterte, J.-E. Otterstedt, *Zeolites* **1994**, *14*, 557–567.
[17] G. Zhu, S. Qui, J. Yu, Y. Sakamoto, F. Xiao, R. Xu, O. Terasaki, *Chem. Mater.* **1998**, *10*, 1483–1486.
[18] S. Mintova, N. H. Olson, V. Valtchev, T. Bein, *Science* **1999**, *283*, 958–960.
[19] R. Van Grieken, J. L. Sotelo, J. M. Menéndez, J. A. Melero, *Microporous Mesoporous Mater.* **2000**, *39*, 135–147.
[20] B.-Z. Zhan, M. A. White, M. Lumsden, J. Mueller-Neuhaus, K. N. Robertson, T. S. Cameron, M. Gharghouri, *Chem. Mater.* **2002**, *14*, 3636–3642.
[21] B. A. Holmberg, H. Wang, J. M. Norbeck, Y. Yan, *Microporous Mesoporous Mater.* **2003**, *59*, 13–28.
[22] R. A. Rakoczy, Y. Traa, *Microporous Mesoporous Mater.* **2003**, *60*, 69–78.
[23] W. Song, R. E. Justice, C. A. Jones, V. H. Grassian, S. C. Larsen, *Langmuir* **2004**, *20*, 8301–8603.
[24] C. S. Cundy, J. O. Forrest, R. J. Plaisted, *Microporous Mesoporous Mater.* **2003**, *66*, 143–156.
[25] Q. Li, B. Mihailova, D. Creaser, J. Sterte, *Microporous Mesoporous Mater.* **2001**, *43*, 51–59.
[26] V. P. Valtchev, A.-C. Faust, J. Lézervant, *Microporous Mesoporous Mater.* **2005**, *68*, 91–95.
[27] J. Aguado, D. P. Serrano, J. M. Escola, J. M. Rodriguez, *Microporous Mesoporous Mater.* **2004**, *75*, 41–49.
[28] C. Baerlocher, W. H. Meier, D. H. Olson, *Atlas of Zeolite Frameworks Types, 5th revised ed.*, Elsevier, Amsterdam, **2001**, p. 266.
[29] L. M. Parker, D. M. Bibbly, *Zeolites* **1983**, *3*, 8–11.
[30] S. A. I. Barri, G. W. Smith, D. White, D. Young, *Nature* **1984**, *312*, 533–534.
[31] R. M. Highcock, G. W. Smith, D. Wood, *Acta Crystallogr. Sect. C* **1985**, *41*, 1391–1394.
[32] A. Araya, B. M. Lowe, *Zeolites* **1984**, *4*, 280–286.
[33] G. T. Kokotailo, J. L. Schlenker, F. G. Dwyer, E. W. Valyocsik, *Zeolites* **1985**, *5*, 349–351.
[34] B. Marler, *Zeolites* **1987**, *7*, 393–397.
[35] C. A. Fyfe, G. T. Kokotailo, H. Strobl, C. S. Pasztor, G. Barlow, S. Bradley, *Zeolites* **1989**, *9*, 531–534.
[36] P. J. Hogan, T. V. Whittam, J. J. Birtill, A. Stewart, *Zeolites* **1984**, *4*, 275–279.
[37] S. Ernst, J. Weitkamp, J. A. Martens, P. A. Jacobs, *Appl. Catal.* **1989**, *48*, 137–148.
[38] R. P. Gunawardane, H. Gies, B. Marler, *Zeolites* **1988**, *8*, 127–131.
[39] F. Di Renzo, F. Remoue, P. Massiani, F. Fajula, F. Figueras, T. Des Courrieres, *Zeolites* **1991**, *11*, 539–548.
[40] P. A. Jacobs, J. A. Martens, *Synthesis of High-Silica Aluminosilicate Zeolites*, Elsevier, Amsterdam, **1987**, p. 233.
[41] J. A. Martens, W. Souverijns, W. H. Verrelst, R. F. Parton, G. F. Froment, P. A. Jacobs, *Angew. Chem.* **1995**, *107*, 2726–2728; *Angew. Chem. Int. Ed. Engl.* **1995**, *34*, 2528–2530.
[42] J. A. Martens, W. H. Verrelst, G. Mathys, S. Brown, P. A. Jacobs, *Angew. Chem.* **2005**, *117*, 5833–5836; *Angew. Chem. Int. Ed.* **2005**, *44*, 5687–5690.
[43] M. A. Camblor, A. Corma, S. Valnecia, *Microporous Mesoporous Mater.* **1998**, *25*, 59–74.
[44] M. Derewinski, P. Sarv, A. Mifsud, *Catal. Today* **2006**, *114*, 197–204.
[45] P. A. Jacobs, J. A. Martens, *Pure Appl. Chem.* **1986**, *58*, 1329–1338.

[46] A. C. Larson, R. B. Von Dreele, *General Structure Analysis System (GSAS)*, Los Alamos National Laboratory Report LAUR 86-748, **2000**.
[47] R. Bialek, *Kriber-Kristallographische Berechnungen Manual*, ETH, Zurich, **1991**.
[48] Ch. Baerlocher, A. Hepp, W. M. Meier, *DLS-76 Manual*, ETH, Zurich, **1977**.
[49] D. Balzar, N. Audebrand, M. R. Daymond, A. Fitch, A. Hewat, J. I. Langford, A. LeBail, D. O. Louër, O. Masson, C. N. McCowan, N. C. Popa, P. W. Stephens, B. H. Toby, *J. Appl. Crystallogr.* **2004**, *37*, 911–924.
[50] W. Huybrechts, J. Mijoin, P. A. Jacobs, J. A. Martens, *Appl. Catal. A* **2003**, *243*, 1–13.

Received: June 25, 2007
Published online: September 17, 2007

